Motion and Performance Analysis of An Experimental Model Floating Wind Turbine

David Bonnici[1], Sean Agius[2], Tonio Sant[3], Daniel Micallef[4]

Department of Mechanical Engineering, University of Malta, Malta

[1]MSc Student, [2]Phd Student, [3]Senior Lecturer, [4]PhD Student;

Email: tonio.sant@um.edu.mt; Tel: 00356 2340 2437

Abstract:

Laboratory measurements of the motion and rotor performance of a model floating wind turbine were undertaken under simple wind and wave conditions. The model consisted of a 40cm diameter rotor mounted on a fully submerged cylinder supported vertically by four arms to form a tension leg floater. The laboratory facility involved a low-wind speed straight-through wind tunnel assembled on the water wave generator. The turbine was connected to a DC generator and an electrical variable-resistance load to vary the rotor speed. Tests were undertaken for one fixed wind speed, varying the rotor tip speed ratio and wave conditions. Four different one-dimensional wave conditions were considered, each with a different wavelength and frequency. Sensors were installed to measure the unsteady wave height and surge of the turbine platform. Other sensors were installed to measure the rotor speed and the generator output power.

The measurements show the effects of rotor tip speed ratio and wave condition on the surge motion of the floater. The presence of aerodynamic damping due to the turbine was evident for certain wave conditions. The rotor experienced considerable deviations in the power coefficient characteristics when subjected to waves. The deviations were larger at and above the optimal tip speed ratio.

Good agreement was obtained when the measurements for the power coefficient and surge displacement were compared with those from a simplified mathematical model. The model was based on the Blade-Element Momentum theory for rotor aerodynamics and on the Morison equation for the hydrodynamic forces on the floater.

Nomenclature.

A_f	Cross sectional area of floater m^2	U	Fluid flow velocity, m/s
A_d	Area of actuator disc, m^2	$\dot{U}$	Fluid flow acceleration, m/s^2
BF	Blockage factor	U_h	Velocity of floating platform, m/s
c	Chord length, m^2	U_w	Wind velocity/tunnel speed, m/s
C_D	Drag Coefficient	x	Surge Displacement, m
C_L	Lift Coefficient	x_c	Centre of surge displacement, m
C_M	Inertia Coefficient	x_p	Peak-to-peak surge displacement, m
C_P	Power Coefficient	η_g	Generator Efficiency
$\overline{C_P}$	Mean Power Coefficient	ρ_a	Density of air, kg/m^3
C_T	Thrust Coefficient	Ω	Rotational Speed of turbine, rad/s
F_T	Thrust of turbine, N	λ	Tip Speed ratio
h	Water Depth, m	λ_w	Wavelength, m
H	Wave Amplitude, m	ζ	Phase angle between wave/floater, deg
I	Generator current, A	θ	Pitch angle, deg
R	Radius of turbine, m	τ	Wave period, s
V	Generator voltage, V		

1. Introduction

Floating wind turbines are subject to complex phenomena resulting from the combined actions of the unsteady aerodynamic, hydrodynamic and inertial loads [1, 2, 3]. The challenge in developing these floating wind turbines is to make the turbine itself to remain stable and aerodynamically efficient in spite of the natural environmental conditions. Experiments on model floating turbines under controlled conditions in a laboratory environment provide valuable data, which until today have been very limited. Such experiments remain indispensible for validating computational tools simulating floating turbines, which undoubtly have to treat more complex phenomena than those dealing with offshore turbines with bottom-mounted foundations. This paper presents the first results from an ongoing research at the University of Malta to test model floating wind turbines under simple and controlled conditions in a laboratory wind/wave generating facility. This paper presents the study related to the experimental testing of a wind turbine mounted on a four-legged tension leg platform. The surge motion of the floater and the power coefficient of the rotor were measured under different operating conditions. Finally, the results were compared with those from a new simplified computer model.

2. Experimental Equipment

2.1 The Wind/Wave Generating Facility and Model Floating Turbine

The wind/wave generating facility consisted of a low-speed straight-through wind tunnel assembled on a water wave generator. Different wave conditions could be generated by varying the oscillating frequency of the wave making paddle. The wind tunnel has a circular cross-sectional area equal to 90cm at the test-section while the wave tank is 8m long and 72cm wide. Figure 1 illustrates a schematic diagram of the model floating turbine installed in the wind/wave generating facility. The model wind turbine was mounted on a tension-leg floater consisting of an 8 inch diameter hollow cylinder of length 44cm. This yielded a Blockage Factor of 14.3% for the floater in the wave tank. The buoyant upthrust of the floater was 120N. The floating structure was anchored to the bottom of the tank via four mooring lines which were attached to four arms protruding from the upper part of the platform.

The model floating wind turbine had a 40cm diameter two-blade rotor, resulting in a Blockage Factor of 20%. The hub diameter was equal to 6cm. The blades had a constant chord of 4cm and were manufactured from 1.5mm thick Aluminum flat plates. The blades cross-sectional profile was given a symmetrical aerofoil shape with a file to form a rounded leading edge and a sharp trailing edge. The aerofoil lift and drag characteristics were determined by separate wind tunnel measurements. These aerodynamic properties were later implemented in the mathematical model. These are presented in Graph 1. The blade twist varied linearly from 33.8 deg at r/R=0.1 to 11 deg at the tip. The rotor had a hub diameter equal to 6cm and was fitted to a Maxon© dc generator. The generator was connected across a 26 Ohm peak variable resistor. It was possible to operate the generator at different tip speed ratios by varying the load resistance.

2.2 Measurement Equipment

In order to measure the wave form and the displacement of the floating platform two sensors were constructed. These two sensors consisted of multi-turn potentiometers which were connected to the platform and wave measurement floater. The sensors were calibrated in order to give the displacement in millimeters equivalent to the output voltage from the potentiometers. Also an LEM current sensor was used to measure the output current from the generator. An encoder was directly connected to the output shaft of the generator in order to measure the rotational speed of the turbine. These entire four sensors together with the output voltage from the generator were connected to the data acquisition device where the SCC-68 I/O connector block was used. The data acquisition system was connected to LabVIEW© software. In order to observe the data a frequency of 100Hz was set for the data acquisition system and a sample of one thousand data points was chosen for the experiments. Details of the experimental set up are presented in Figure 2. A pitot-static probe was used in conjunction with an incline tube manometer to measure the tunnel speed.

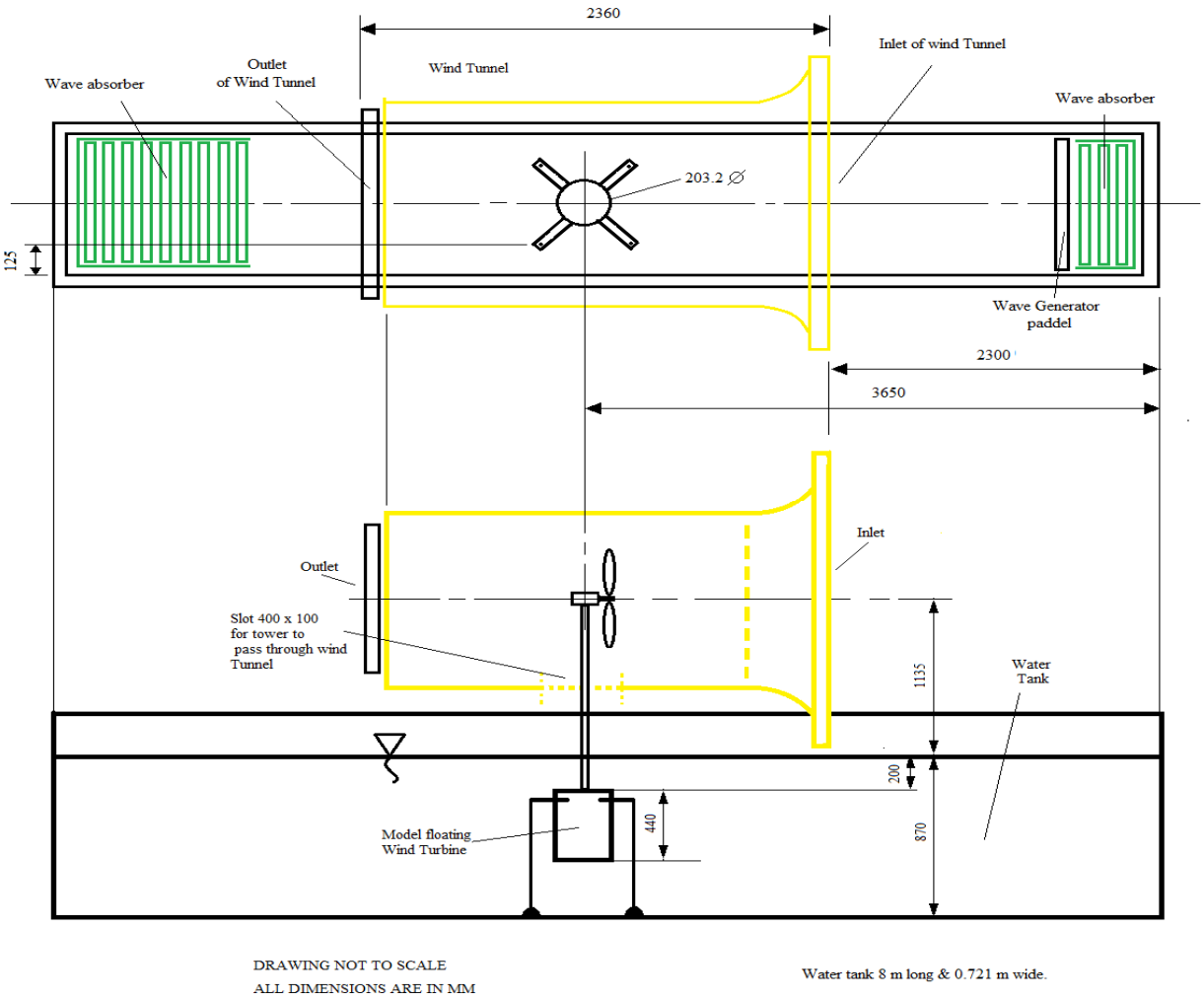

Figure 1: Schematic Diagram

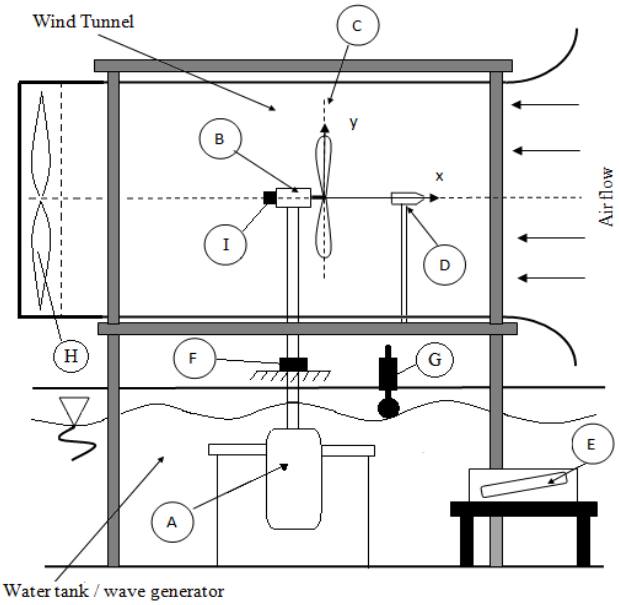

Figure 2: Setup of Apparatus

Legend	Description
A	*Tension leg floating platform.*
B	*Generator and Turbine assembled on tower.*
C	*Rotor plane of rotation.*
D	*Pitot static tube to measure wind speed*
E	*Inclined Manometer to measure pressure difference from the pitot static probe.*
F	*Displacement sensor to measure the surge displacement x of the model floating wind turbine.*
G	*Wave sensor to measure the wave form generated.*
H	*Wind tunnel extraction fan*
I	*Encoder to measure the rotational speed of the turbine.*

Table 1: Blade Geometry

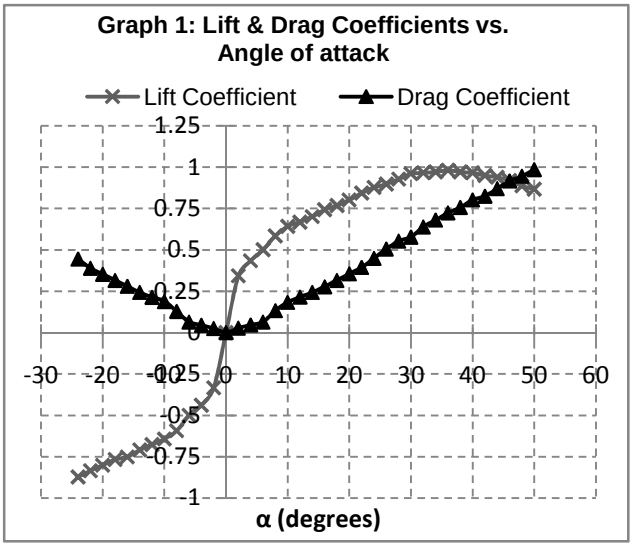

3. Experiments under Static Conditions

Initial experiments on the turbine were carried in order to measure its thrust and power coefficients under static conditions, i.e. no waves and the floater fixed. The wind tunnel speed was kept constant at 12.8m/s while the rotor speed was varied to measure the rotor axial thrust and rotor output power at various tip speed ratios. The thrust F_T was measured using a spring balance while the rotor output power could be determined by measuring the generator voltage (V) and current (I). For each tip speed ratio, the mean and standard deviation were computed based on 1000 sample values for I, V and Ω to be able to find the mean and standard deviation. The values of the thrust and power coefficients were estimated using the following equations:

$$F_T = {}^1/_2\, C_T\, A_d\, U_w{}^2 \quad \text{and} \quad C_P = V \times I / \eta_g \, \frac{1}{2} \rho_a A_d U_w{}^3$$

Since the turbine contains inefficiencies due to the rotor and the d.c generator, the term η_g referring to the generator efficiency was introduced in the equation in order to obtain the power coefficient for the rotor. The efficiency of the generator at different rotational speeds was measured in a separate experiment. The C_T-λ and C_P-λ curves for static conditions are shown in Graphs 2 and 3 below. An error analysis was undertaken. The error bars shown in the graph below show the one plus/minus standard deviations in the derived thrust and power coefficients.

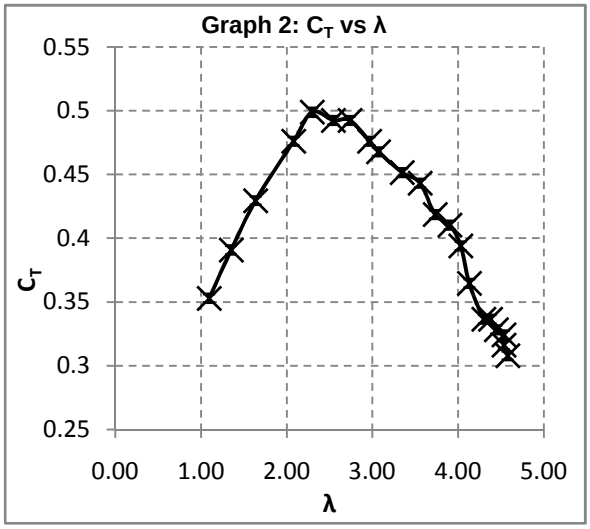

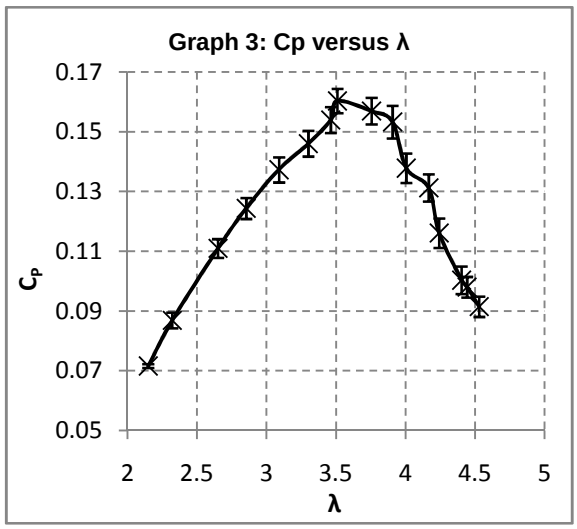

4. Experimental Campaign with the Model Subjected to Waves

The model floating turbine was tested under four different wave conditions which are indicated in Table 2. Under such conditions, one dimensional non-breaking intermediate/deep water waves were created (see Figure 4). The measurements were conducted with a fixed wind tunnel speed of 12.8m/s. The rotor speed was varied by altering the resistance of the electrical load connected to the generator. Two different experiments were conducted: In the first experiment, the unsteady surge motion of the floating system was measured for different wave settings and rotor tip speed ratios. The second experiment was aimed at measuring the instantaneous rotor power coefficient.

Table 2: Wave Properties.

Wave	Inverter frequency (Hz)	Wavelength λ (m)	Amplitude H(m)	Wave frequency (Hz)	$\frac{H}{g\tau^2}$	$\frac{h}{g\tau^2}$
1	21.6	2.2	0.025	0.70824	0.00128	0.044
2	23,5	2	0.026	0.7703	0.00157	0.053
3	27	1.8	0.028	0.8849	0.00223	0.069
4	30	1.5	0.033	0.9868	0.00327	0.086

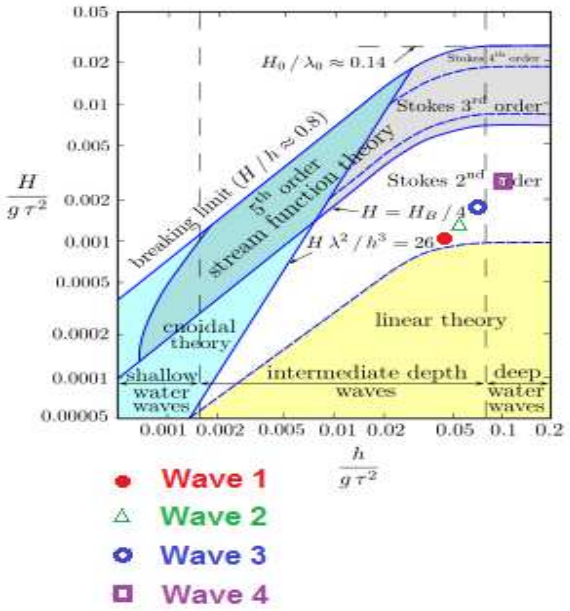

Figure 4: Limits of validity for selected wave theories. Source [4].

4.1 Motion Analysis

Graph 4 shows the variation of the maximum forward and aft surge displacement with tip speed ratio for the four different wave conditions. The uncertainty in the displacement results was ± 0.5 mm. The maximum variation in the rotor speed was estimated to be equal to 0.56% (percentage maximum standard deviation divided by mean). From Graphs 2 and 4, it is evident that the rotor axial thrust coefficient, and hence also λ, have a considerable influence on the surge motion. The rotor aerodynamic force displaced the platform backwards up to a tip speed ratio of around 3.

Graph 5 shows the corresponding values for the peak-to-peak displacement of the oscillation of the floater. This was estimated from the difference between the maximum forward and aft displacement. For wave 1, the peak-to-peak displacement exhibited a notable dependence on the tip speed ratio. The largest values were observed when the rotor was not rotating (i.e. at λ=0) and at high tip speed ratios. The displacement decreased at tip speed ratios ranging between 1 and 3.4. Evidently this behaviour is a result of the aerodynamic damping created by the rotor. For wave

conditions 2, 3 and 4, x_p remained relatively constant with λ. This is mainly due to the fact that hydrodynamic forces on the floater resulting from such waves were significantly larger than the rotor aerodynamic thrust and consequently aerodynamic damping had little influence on the surge peak-to-peak motion.

Graph 6 shows how the initial centre of oscillation varied with tip speed ratio for different wave conditions. The analysis shows that the centre of oscillation for each particular tip speed ratio remained almost the same when the platform was subjected to different waves. The maximum observed variation in x_c when varying the wave conditions was only of 7 mm. This was significantly smaller than the corresponding variation in x_p for the same wave conditions.

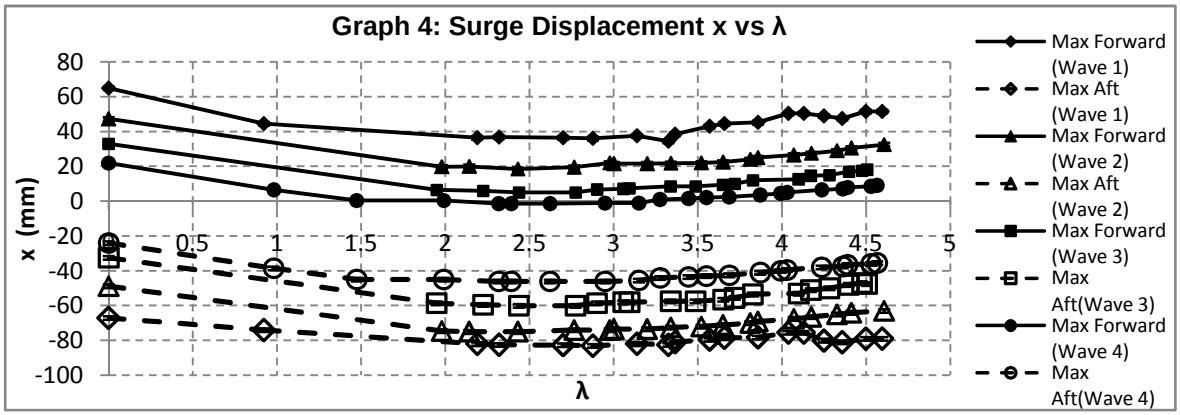

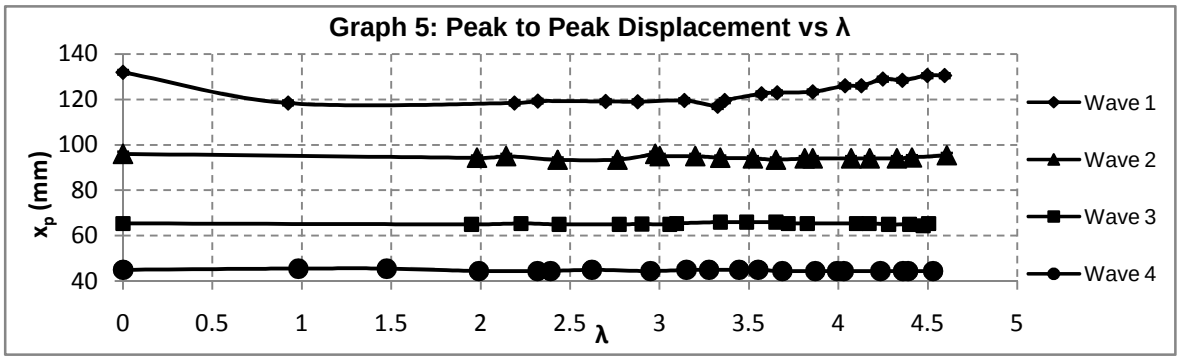

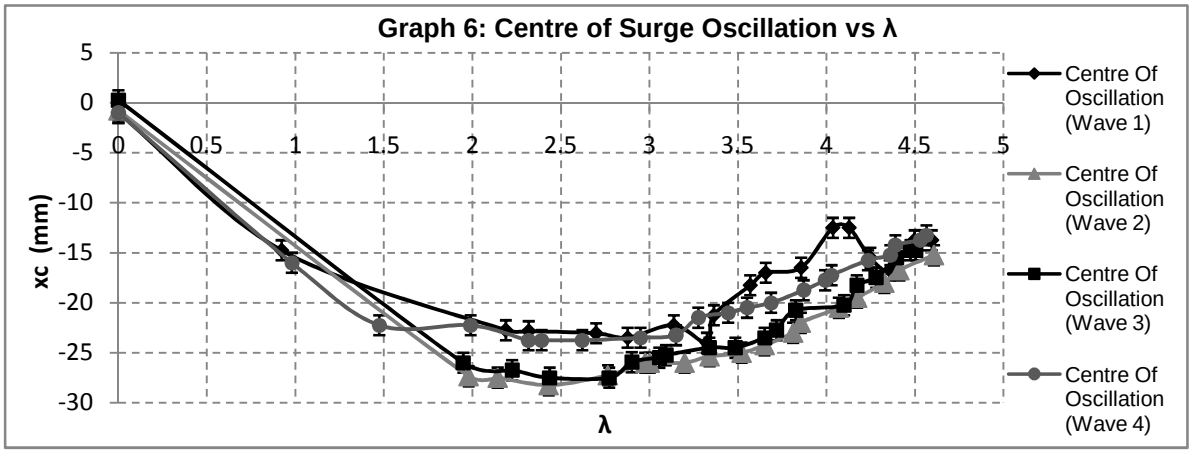

Graph 7 shows how the phase angle ζ between tip of the wave crest and the maximum surge displacement of the platform varied with the tip speed ratio for the four different wave conditions. The phase angle ζ generally increased with larger tip speed ratios. As expected, the wave conditions were found to have a significant effect on the phase angle at all tip speed ratios.

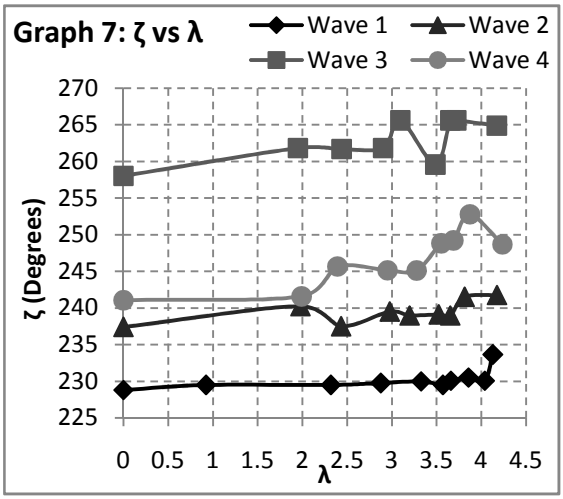

4.2 Performance Analysis

With the data acquisition available, it was possible to measure the instantaneous power coefficient of the turbine with time for the four wave conditions. When the platform is subjected to waves the wind flow across the rotor is continuously changing relative to the platform velocity. Therefore since the C_P and λ are a function of the wind velocity U_h, then both the power coefficient and the tip speed ratio will change continuously with time depending on the platforms velocity U_h. Hence, at a given time, values of C_P and λ will become:

$$C_P = \frac{\text{Power}}{{}^1/_2\,\eta_g g A_d\,\rho_a (U_w + U_h)^3} \qquad \lambda = \frac{R\Omega}{U_w + U_h}$$

Plotting the instantaneous values of C_P versus λ resulted in a cloud of data points for different load conditions on the generator. The results for Wave 1 are shown in graph 8. The rotor speed remained practically constant during the wave action (maximum variation less than 1%). Thus the variations in C_P and λ were mainly associated with fluctuations in the U_h. The maximum and minimum deviations of C_P obtained from static conditions are represented by the dotted line of Graph 8. From the same graph it was noted that the deviations in C_P from the mean curve were larger when the platform was subjected to waves than in static conditions (no surge). This increase was more evident when λ was larger than three.

Graphs 9 shows the C_P vs λ curve when the model floating wind turbine was subjected to the four wave conditions. Only the mean values are plotted ($\overline{C_P}$). The curve for static conditions is also included. It may be easily observed that for low tip speed ratios, at which the wind turbine is expected to experienced stalled conditions, the mean power coefficient was almost unaffected by the platform motion. On the other hand, $\overline{C_P}$ became sensitive to the wave actions for values of λ higher than 3. In fact, a decrease in the optimal value for $\overline{C_P}$ was observed at all wave conditions. It is clear that wave behaviour has a considerable influence on the operating power coefficient for a floating wind turbine. The level of influence depends on the tip speed ratio at which the rotor is operated.

5. Mathematical Model.

A simplified mathematical model for the floating wind turbine on a TLP system was implemented in a computer program to predict in the time domain the platform surge and rotor performance. The model is based on the following:

- The Blade Element Momentum (BEM) Theory for modelling the rotor aerodynamics. The effects of dynamic inflow on the wake as well as those related to stall delay and dynamic stall phenomena on the blades are ignored.

- The Morison equation for determining the unsteady hydrodynamic forces on hull, platform arms and mooring lines due to sea currents and waves. The following form of the Morison equation is implemented :

$$F(t) = \rho C_M(\mathrm{v_h})\dot{u} + \frac{1}{2}\rho C_D(A_f)(u)|u|$$

  The first term is due to inertia effects while the second term is due to the drag. $F(t)$ is the time dependent total force generated on the body due to the incoming waves; *v* is the volume of the structure being considered; $\dot{u}$ and u are the wave particle acceleration and velocity at a particular time instant, which are found by using Linear Airy's or Stokes's theory in conjunction with Figure 4, and A_f is the frontal area of the structure.
- The wind turbine blades and tower are assumed to be rigid. The stretching of the tension legs is however taken into account.

A time-marching algorithm using a Runge Kutta solver is implemented to obtain the response of the floating systems (displacement, velocity and acceleration) as a function of time. With each time step, the code computes the effective forces together with the mass, added mass, damping and stiffness of the structure. The new displacement is calculated and when the structure moves, the tension in the moorings increases to produce higher stiffness. Thus, the system response is updated and recalculated with this new stiffness. This procedure is repeated until the displacement and the stiffness converge and equilibrium is reached. Likewise, since the forces produced by the wave on the hull depend on the distance moved by the structure, the wave forces are recalculated until convergence is achieved. The geometry and buoyancy of the structure are updated by the recalculation of the vertical displacement. This is iterated until overall convergence is attained.

The C_P vs λ curve predicted by the mathematical model for the tested two-bladed rotor under static conditions (no waves and surge motion) is shown in Graph 10. For this computation, the static aerofoil data presented in Graph 1 were used. A reasonably good agreement with the experimental results was obtained. Graph 11 compares the peak-to-peak surge displacement of the platform from the simulation with the corresponding experimental results for Wave 1 conditions. The mathematical model predicts this displacement very accurately at the optimal range of tip speed ratios (for 2.2 < λ <3.80).

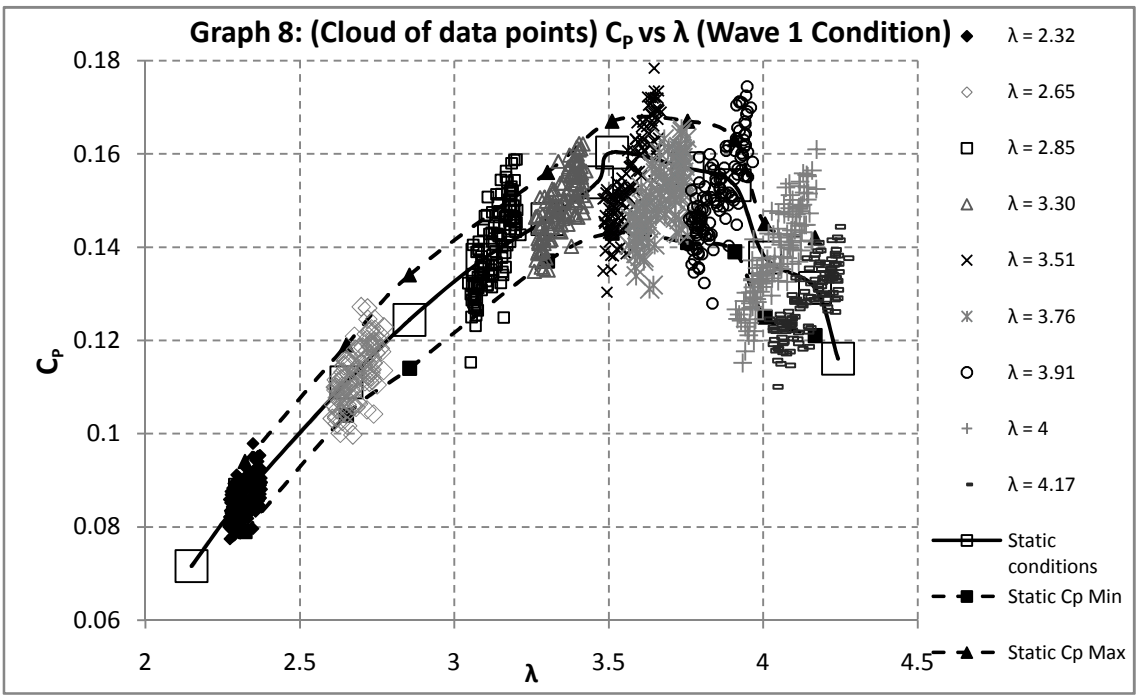

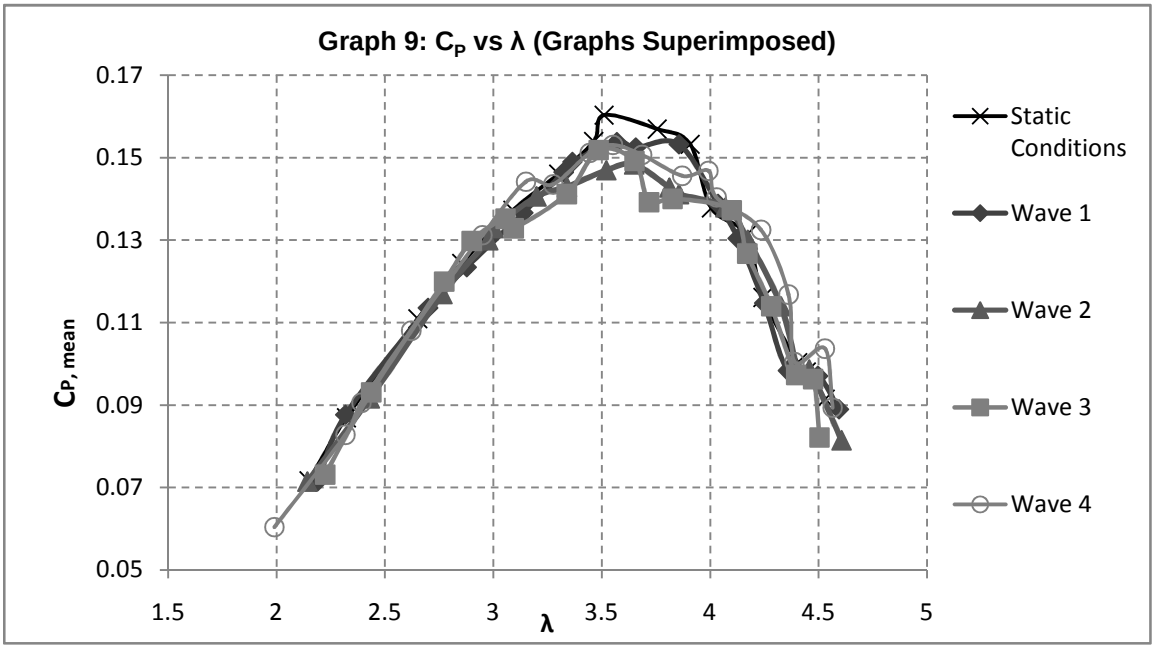

At higher tip speed ratios than the optimal value, the simulation under-predicts the peak to peak displacement. The most probable cause is the deficiency of the BEM theory implemented in simulating the rotor loads at higher tip speed ratios. This is in fact also evident in the Graph 12 for the power coefficient. It confirms the importance of having reliable aerodynamic models for simulating the dynamics of floating wind turbines.

Graph 12 shows the results obtained for the mean power coefficient for $\overline{C_P}$ when the model floating wind turbine was subjected to Wave 1 condition. Graph 13 presents the corresponding maximum and minimum values for C_P as predicted by the simulation. It is noted that the largest fluctuation (Max-Min) is more prominent at higher tip speed ratios. This behaviour is consistent with what was observed in the measurements (Graph 8).

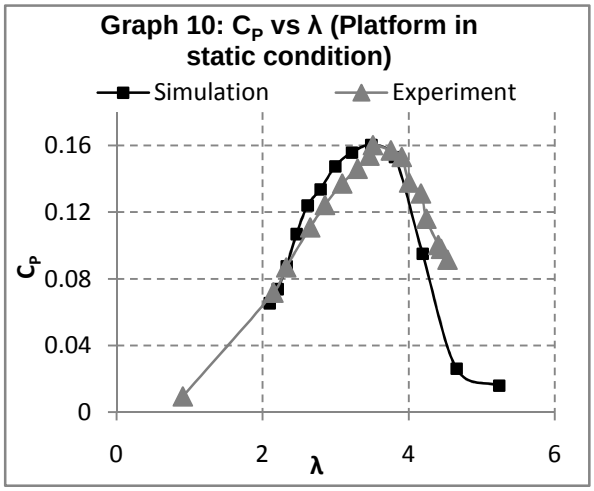

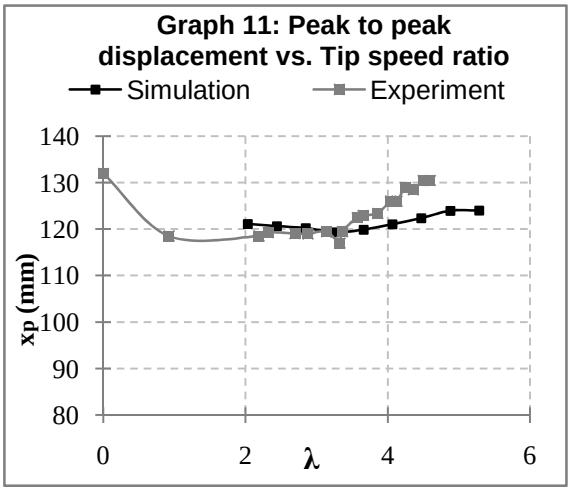

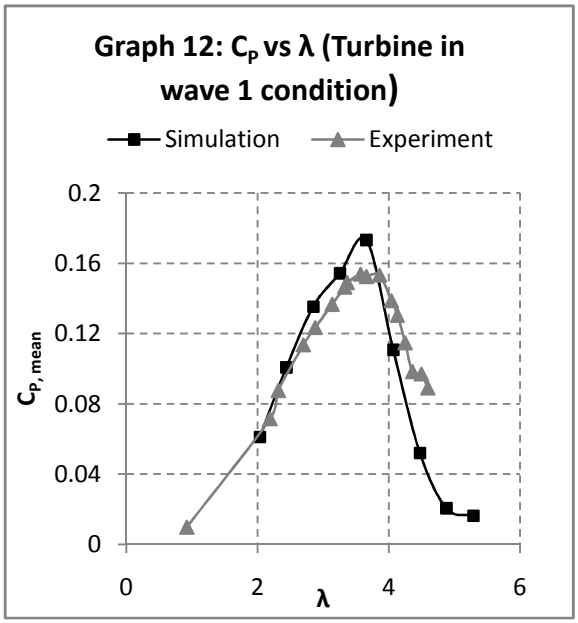

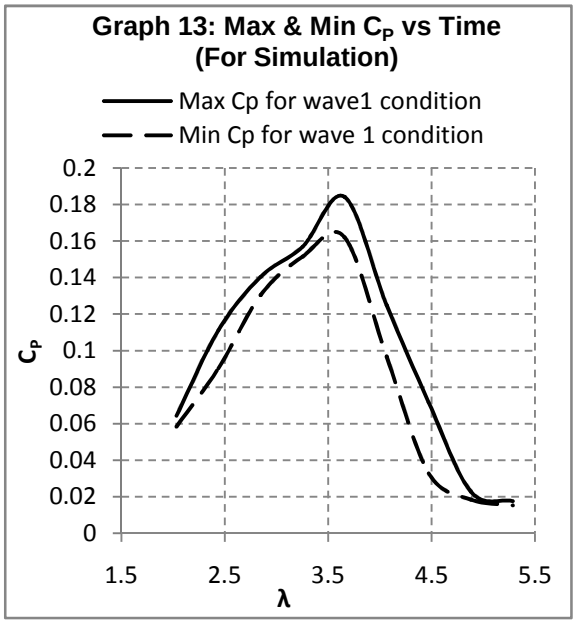

6. Conclusion

A small model floating wind turbine on a TLP platform was tested in a wind/wave generating facility under simple and controlled conditions. The surge displacement and power coefficient were measured for different wave conditions using a data acquisition system with a high sampling frequency. It was possible to measure the platform's motion at any instance relative to the initial rest position of the floating structure. The analysis also provided more information on how the operating power coefficient of a floating wind turbine fluctuates under the effect of wave motion. The presented results provide valuable data for validating simulation tools for floating wind turbines.

The experiments examined the influence of rotor aerodynamics and wave hydrodynamics on the surge displacement of the floating system. The presence of rotor aerodynamic damping from the rotor could be noted, but its influence on surge motion was found to be highly dependent on the wave conditions and rotor operating tip speed ratio.

The power coefficient of the turbine subjected to wave action deviated considerably from that measured under static (no surge) conditions. The deviations were more pronounced at higher tip speed ratios. It was also noted that platform oscillations led the turbine to suffer from an appreciable loss in its optimal power coefficient. The same behaviour was observed in the results predicted by a simplified mathematical model. Further work is however required to clearly establish the physical reasons for such behaviour and how this will vary for different rotor geometries.

7. References

[1] Sebastian T, Lackner M A. *Offshore Wind Turbines - An Aerodynamic perspective.* University of Massachusettes.

[2] Jonkman J.M., *Dynamic Modeling and Loads analysis of an Offshore Floating Wind turbine,* US Department of Energy, 2007.

[3] Withee J.E, *Fully Coupled Dynamic Analysis of a Floating Wind Turbine*, Massachusettes Institute of Technology, 2004.

[4] Le Mehaute B., *An Introduction to Hydrodynamics and Water Waves*" Environmental Science Services Administration, Pacific Oceanographic Laboratories, Miami, Essa Technical Report ERL 118-POL-3-2 1969.